JETIR.ORG ISSN: 2349-5162 | ESTD Year : 2014 | Monthly Issue
JOURNAL OF EMERGING TECHNOLOGIES AND INNOVATIVE RESEARCH (JETIR)
An International Scholarly Open Access, Peer-reviewed, Refereed Journal

A Compact Dual-Band Implantable Antenna for Biomedical Applications

[1]Polnati Gowthami, [2]Rama Devi Kolisetty
[1]PG Student, [2] Associate Professor, Department of Electronics and Communication Engineering
University College of Engineering, JNTU Kakinada, Andhra Pradesh, India

ABSTRACT

This paper presents a compact dual-band implantable antenna for biomedical wireless communication applications. The antenna consists of a slot-loaded radiating patch, ground plane, dielectric substrate, protective superstrate, and coaxial probe feed. Rogers RT/duroid 6010 with a relative permittivity of 10.2 and loss tangent of 0.0023 is used as the dielectric material. The design is developed in two stages. Initially, a 4.6 × 4.6 × 0.26 mm³ antenna is analyzed in free space to obtain its baseline response. The antenna is then reduced to 4 × 4 × 0.26 mm³ for tissue-loaded analysis. Four tissue phantom models, namely heart, stomach, small intestine, and large intestine, are considered. For the small-intestine phantom, the antenna operates near 1.39 GHz and 2.46 GHz, with simulated −10 dB bandwidths of 67 MHz and 121 MHz, respectively. The effects of tissue loading are studied using S11 characteristics, radiation patterns, realized gain, and surface-current distribution. The results show that the surrounding tissue affects the resonant frequency and impedance matching while maintaining dual-band operation. The proposed antenna is investigated using Ansys HFSS and provides a compact structure suitable for numerical study of implantable biomedical communication systems. Fabrication, measurement, efficiency verification, and SAR analysis are considered for future work.

.**Index Terms—Implantable antenna; dual-band antenna; biomedical communication; Rogers RT/duroid 6010; tissue phantom; HFSS; compact antenna.**

I. INTRODUCTION

Implantable antennas play an important role in biomedical wireless communication systems, where a small antenna is required to establish a wireless link between an implanted device and an external reader. The limited space available inside the human body and the different electromagnetic properties of biological tissues make the design of such antennas challenging. In particular, tissue loading can influence the resonant behaviour and impedance characteristics of the antenna.

The present work focuses on a compact dual-band implantable antenna designed using a slot-loaded radiating patch. The slot modifies the effective current path and enables dual-band operation while maintaining a small antenna footprint. The design is developed in two stages. Initially, a 4.6 × 4.6 × 0.26 mm³ antenna is analyzed in free space. The antenna is subsequently reduced to 4 × 4 × 0.26 mm³ for tissue-loaded analysis. The structure consists of a ground plane, dielectric substrate, slot-loaded radiating patch, protective superstrate, and coaxial probe feed.

The overall concept of the proposed work is shown in Fig. 1. It illustrates the placement of the implantable antenna within the body and its wireless communication link with an external reader. The enlarged antenna view shows the main structural layers, namely the superstrate, radiating patch, substrate, ground plane, and coaxial feed. The figure also presents the four tissue phantoms environments considered in the study: heart, stomach, small intestine, and large intestine.

The proposed antenna is modelled and analyzed using Ansys HFSS under free-space and tissue-loaded conditions. The study examines the antenna response in terms of resonant behaviour, impedance characteristics, bandwidth, radiation patterns, realized gain, and surface-current distribution.

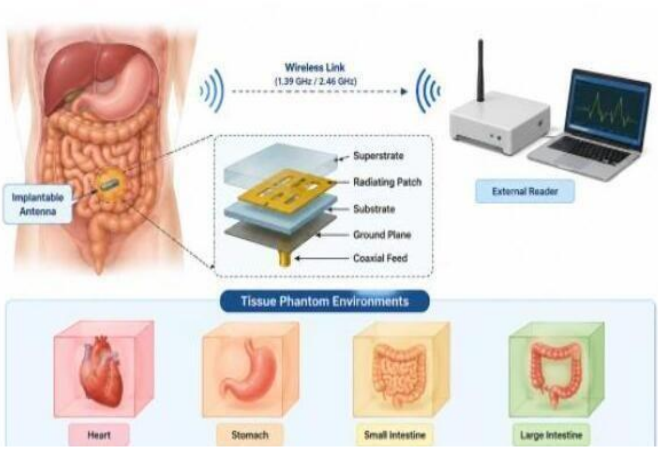

Fig. 1. Conceptual representation of the proposed implantable antenna, wireless link with the external reader, antenna structure, and tissue phantom environments.

II. PROPOSED ANTENNA DESIGN

A.Free-Space Antenna Design

The initial antenna is designed for free-space analysis with an overall size of 4.6 × 4.6 × 0.26 mm³ using a slot-loaded radiating patch, substrate, superstrate, ground plane, and coaxial probe feed. The top view in Fig. 2(a) shows the rectangular patch with the slot arrangement and circular feed-related features, while the 3D view in Fig. 2(b) illustrates the complete layered structure and the coaxial probe extending from the lower side. Rogers RT/duroid 6010 is used for the substrate and superstrate with $\varepsilon r = 10.2$ and tan $\delta = 0.0023$. This configuration is modelled in Ansys HFSS and serves as the initial reference design before the antenna is reduced for tissue-phantom analysis.

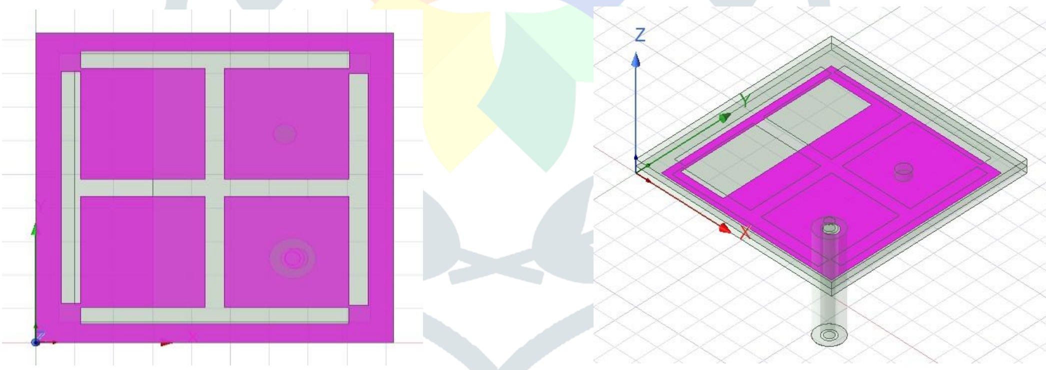

Fig. 2. Free-space antenna geometry: (a) top view and (b) 3D view of the proposed antenna.

B. Tissue-Loaded Antenna Design

The antenna is further reduced to an overall size of 4 × 4 × 0.26 mm³ for tissue-phantom analysis. The design retains the slot-loaded patch and coaxial probe feeding arrangement, while the compact dimensions are adjusted for the tissue-loaded condition. Fig. 3(a) shows the top view of the modified radiating structure and its slot arrangement, while Fig. 3(b) presents the corresponding groundplane configuration. Fig. 3(c) shows the side view of the antenna, indicating the substrate and superstrate thicknesses. The final structure is modelled in Ansys HFSS and subsequently placed within the selected tissue phantom environments for simulation.

Fig. 3. Tissue-loaded antenna geometry: (a) top view of the radiating patch, (b) ground-plane view, and (c) side view showing the substrate and superstrate layers.

C. Design Parameters

The final antenna dimensions and feeding parameters used in the HFSS model are summarized in Table 1. The compact 4 × 4 × 0.26 mm^3 configuration is obtained by reducing the initial free-space design while retaining the required slot and feeding arrangement. These parameters are used for the subsequent tissue-phantom simulations.

Table 1. Design Parameters of the Proposed Antenna

Parameter	Value [mm]
Antenna length, L	4.0
Antenna width, W	4.0
Substrate thickness, h_1	0.13
Superstrate thickness, h_2	0.13
Ground length, Lg	4.0
Ground width, Wg	4.0
Central slot length	3.3
Central slot width	0.15
Coaxial feed height, Cr	0.84
Pin diameter	0.30
Port diameter	0.60

D. Governing Design Equations

The initial dimensions were obtained from standard microstrip-patch relations [17] and then adjusted through full-wave optimization in HFSS. This refinement accounts for the effects of the slot geometry, multilayer arrangement, feed position, and the dielectric loading introduced by the surrounding tissue. The governing relations used to establish the initial patch dimensions are given below.

Effective Dielectric Constant

The effective dielectric constant accounts for the effect of the dielectric substrate and the fringing fields around the patch. It is given by:

$$\varepsilon_{eff} = \frac{\varepsilon_r+1}{2} + \frac{\varepsilon_r-1}{2}\left(1 + 12\frac{h}{W}\right)^{-1/2} \quad (1)$$

Effective Patch Length

The effective resonant length of the patch can be estimated using:

$$L_{eff} = \frac{c}{2 f_r \sqrt{\varepsilon_{eff}}} \quad (2)$$

Fringing-Field Extension

The electromagnetic fields extend slightly beyond the physical edges of the patch. The additional length caused by this fringing effect is calculated using:

$$\Delta a = 0.412h \frac{(\varepsilon_{eff}+0.33)\left(\frac{a}{h}+0.264\right)}{(\varepsilon_{eff}-0.258)\left(\frac{a}{h}+0.8\right)} \quad (3)$$

Actual Patch Length

The physical patch length can then be obtained from:

$$L = L_{eff} - 2\Delta L \quad (4)$$

III. SIMULATION METHODOLOGY

The proposed antenna is analyzed using the full-wave finite-element solver in Ansys HFSS. The initial 4.6 × 4.6 × 0.26 mm³ antenna is first simulated in free space to obtain the reference response. The reduced 4 × 4 × 0.26 mm³ antenna is then used for tissue-phantom analysis. A frequency sweep is performed over the two operating regions, with adaptive mesh refinement applied near the upper operating frequency. An open radiation boundary of approximately 40 × 40 × 40 mm³ and a 50 Ω coaxial feed are used in the simulation model.

For the main analysis, the antenna is placed at the centre of a homogeneous 20 × 20 × 20 mm³ tissue block. Four tissue models heart, stomach, small intestine, and large intestine are considered by assigning their respective dielectric properties. The relative permittivity and electrical conductivity values used at the two operating frequencies are listed in Table 2.

Table 2. Dielectric Properties of the Simulated Tissue Phantoms at the Two Resonant Frequencies

Tissue	εr at 1.39 GHz	σ (S/m) at 1.39 GHz	εr at 2.46 GHz	σ (S/m) at 2.46 GHz
Heart	57.5	1.51	54.8	2.26
Stomach	63.9	1.44	62.2	2.21
Small intestine	57.1	2.44	54.4	3.17
Large intestine	56.1	1.33	53.9	2.03

Table 2 [22]represents the different electromagnetic loading conditions of the selected tissues. Among these models, the smallintestine phantom is used for detailed analysis of the antenna characteristics. The simulations are used to obtain S11, resonant frequency, impedance bandwidth, radiation patterns, realized gain, and surface-current distribution.

IV. RESULTS AND DISCUSSION

A.Free-Space Analysis of the Initial Antenna

The initial 4.6 × 4.6 × 0.26 mm³ antenna is first analyzed under free-space conditions to establish its reference response. Fig. 4 shows the simulated S11 characteristics, where two distinct resonances are observed at 1.435 GHz and 2.710 GHz, with minimum S11 values of −22.49 dB and −29.79 dB, respectively. The obtained dual-resonant response confirms that the slot-loaded configuration supports two operating bands within the compact antenna structure. The corresponding impedance bandwidths are considered using the −10 dB criterion.

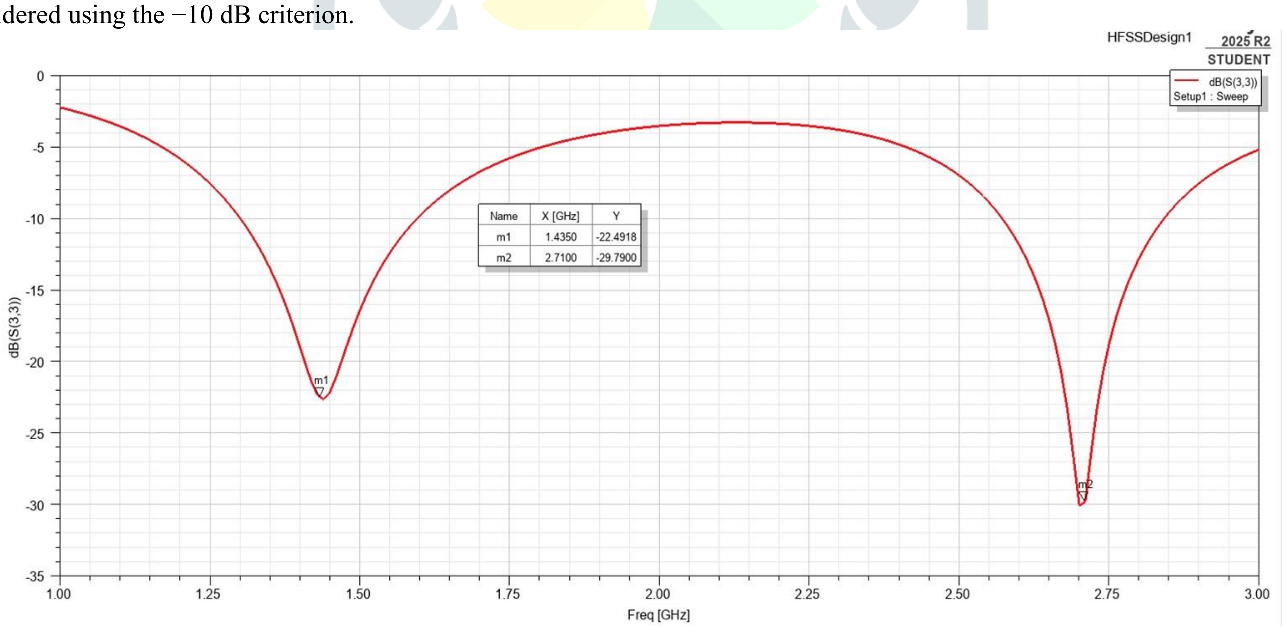

Fig. 4. Simulated S11 characteristics of the initial 4.6 × 4.6 × 0.26 mm³ antenna in free space.

B. Tissue-Phantom Analysis

The reduced 4 × 4 × 0.26 mm³ antenna is next evaluated under different tissue-phantom environments. Fig. 5(a) compares the simulated S11 responses for heart, stomach, small intestine, and large intestine, showing that the surrounding tissue influences the antenna resonance and impedance characteristics. Among these cases, the small-intestine phantom is selected for detailed analysis. As shown in Fig. 5(b), the antenna exhibits two resonant frequencies at 1.39 GHz and 2.46 GHz, with S11 values of −10.62 dB and

−10.70 dB, respectively. The obtained response confirms the dual-band operation of the reduced antenna under the selected tissueloading condition.

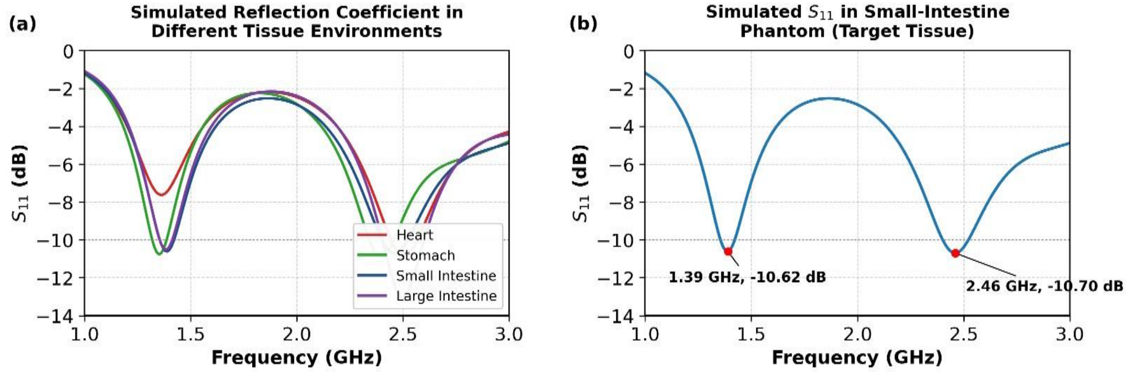

Fig. 5. Simulated S11 characteristics of the tissue-loaded antenna: (a) comparison for different tissue environments and (b) detailed response in the small-intestine phantom.

C. Comparison of Free-Space and Tissue-Loaded Responses

Table 3 summarizes the resonant frequencies, S11 values, and −10 dB impedance bandwidths of the antenna under free-space and different tissue-phantom conditions. The free-space configuration represents the initial 4.6 × 4.6 × 0.26 mm³ design, while the phantom cases correspond to the reduced 4 × 4 × 0.26 mm³ antenna. The results show a shift in the resonant frequencies after introducing the tissue environment, indicating the influence of the surrounding biological medium on the antenna response. Among the considered phantom models, the small-intestine case provides resonances at 1.39 GHz and 2.46 GHz, with S11 values of −10.62 dB and −10.70 dB, respectively.

Table 3. Resonant Frequencies, S_{11} and Bandwidths with and without Tissue Phantoms

Antenna Placed		f_1 (GHz)	S_{11} at f_1 (dB)	Band Width(MHz)	f_2 (GHz)	S_{11} at f_2 (dB)	Band Width(MHz)
In Free Space(without phantom)		1.43	-22.49	200	2.71	-29.79	180
In Different Phantom Types	Heart	1.36	−7.63	-	2.50	−10.85	124
	Stomach	1.35	−10.76	67	2.40	−10.94	116
	Small intestine (target)	1.39	−10.62	67	2.46	−10.70	121
	Large intestine	1.38	−10.52	60	2.50	−13.05	196

D. Radiation Pattern, Gain, and Surface-Current Behaviour

The radiation characteristics for the small-intestine phantom are shown in Fig. 6. At 1.39 GHz, the E-plane and H-plane cuts in Fig. 6(a) and Fig. 6(c) show broad radiation lobes, whereas the corresponding 2.46 GHz cuts in Fig. 6(b) and Fig. 6(d) become more directional and exhibit a figure-eight type distribution. These changes indicate that the radiation pattern is frequency dependent and that the tissue-loaded antenna excites different current modes at the two resonances.

The three-dimensional realized-gain plots in Fig. 6(e) and Fig. 6(f) provide the spatial form of the same radiation response. The lower-frequency pattern spreads over a wider angular region, while the upper-frequency pattern is more concentrated. The simulated peak realized gains are approximately −15.8 dB at 1.39 GHz and −21.4 dB at 2.46 GHz in the small-intestine phantom.

The lower realized gain at 2.46 GHz is consistent with the stronger electromagnetic loss introduced by biological tissue at the higher frequency. In addition, Fig. 6(g) gives the simulated surface-current distribution, which helps relate the observed resonances to the physical current paths on the patch.

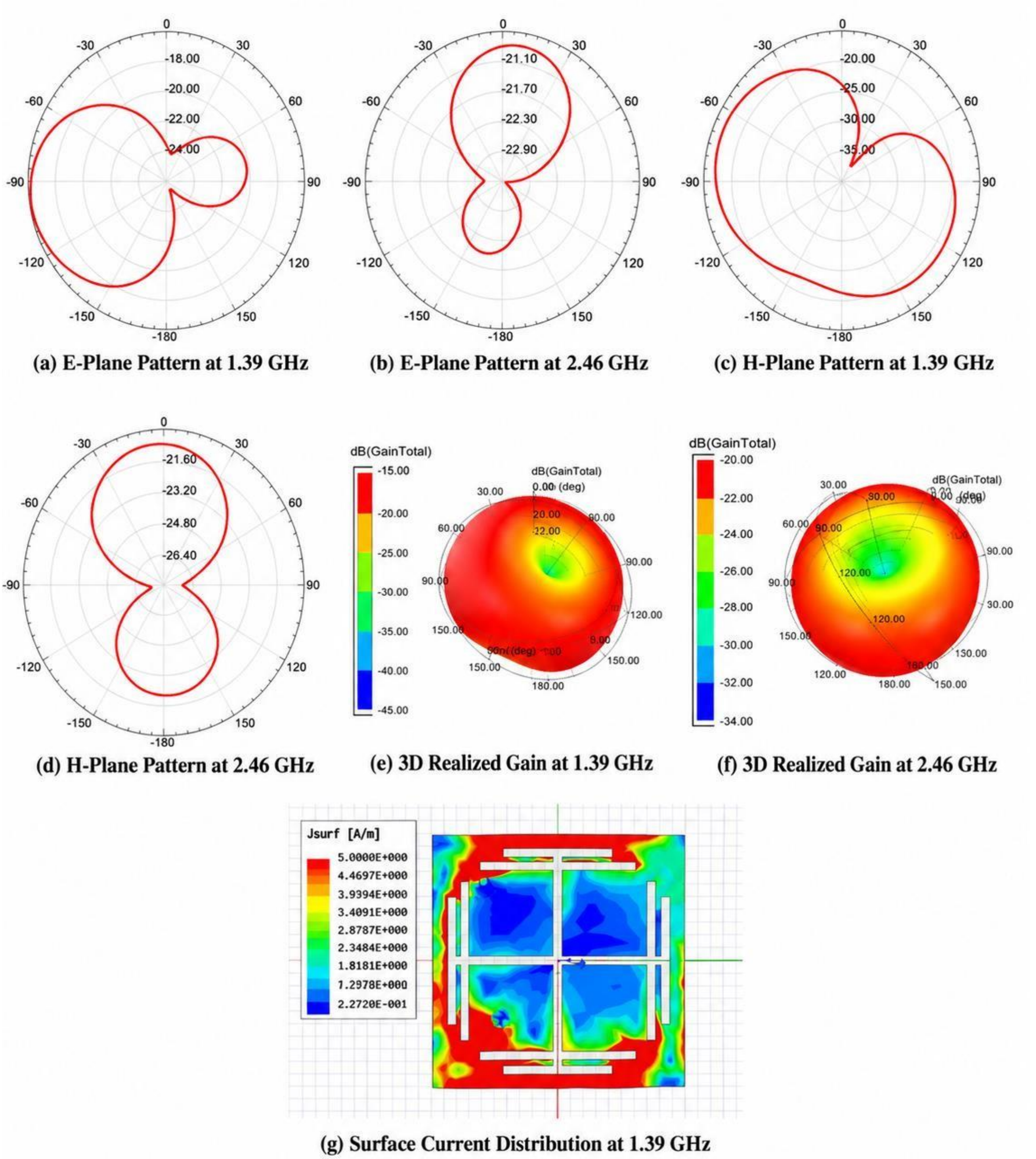

Fig. 6. Simulated radiation characteristics in the small-intestine phantom: (a) E-plane pattern at 1.39 GHz; (b) E-plane pattern at 2.46 GHz; (c) H-plane pattern at 1.39 GHz; (d) H-plane pattern at 2.46 GHz; (e) 3D realized gain at 1.39 GHz; (f) 3D realized gain at 2.46 GHz; and (g) surface current distribution at 1.39 GHz.

The surface-current plot in Fig. 6(g) shows stronger current concentration along the outer patch boundary and the slot sections close to the feed, while the regions enclosed by the slots carry comparatively lower current. The slot arrangement therefore increases the effective electrical path and contributes to the lower-frequency resonance, while the separate current paths around the slot edges support the second resonance. The current distribution also indicates that the feed-adjacent region is important for impedance tuning.

E. Overall Performance Summary

The proposed antenna demonstrates dual-band operation in both the initial free-space and final tissue-loaded configurations. The initial 4.6 × 4.6 × 0.26 mm³ design exhibits resonances at 1.435 GHz and 2.710 GHz, while the reduced 4 × 4 × 0.26 mm³ antenna shows tissue-dependent resonant behaviour around 1.35–1.39 GHz and 2.40–2.50 GHz. Among the considered tissue environments, the small-intestine phantom provides resonances at 1.39 GHz and 2.46 GHz with S11 values of −10.62 dB and −10.70 dB, respectively. These results demonstrate that the compact slot-loaded configuration maintains dual-band operation while its response changes with the surrounding tissue environment.

V. CONCLUSION

A compact dual-band implantable antenna for biomedical wireless communication applications has been designed and analyzed using Ansys HFSS. The antenna employs a slot-loaded radiating patch with a compact multilayer structure and coaxial probe feeding. The design was developed in two stages, where the initial $4.6 \times 4.6 \times 0.26$ mm³ configuration was evaluated in free space, followed by a reduced $4 \times 4 \times 0.26$ mm³ configuration for tissue-phantom analysis. Four tissue environments, namely heart, stomach, small intestine, and large intestine, were considered. The small-intestine phantom exhibited dual resonances at 1.39 GHz and 2.46 GHz, with S11 values of −10.62 dB and −10.70 dB, respectively. The radiation characteristics and surface-current distribution were also investigated to understand the behaviour of the antenna under tissue loading.

The comparison between the free-space and tissue-loaded configurations shows the influence of the surrounding biological medium on the resonant response and impedance characteristics of the antenna. Despite the dimensional reduction and tissue loading, the proposed structure maintains its compact form and dual-band behaviour, demonstrating its potential for numerical investigation in implantable biomedical communication systems. The present work is limited to full-wave HFSS simulations; therefore, fabrication, experimental measurement, SAR evaluation, radiation-efficiency verification, and practical validation are considered as important future work.

REFERENCES

[1] S. Movassaghi, M. Abolhasan, J. Lipman, D. Smith, and A. Jamalipour, "Wireless body area networks: A survey," IEEE Commun. Surveys Tuts., vol. 16, no. 3, pp. 1658–1686, Third Quarter 2014.

[2] S. Kiani, P. Rezaei, and M. Fakhr, "A CPW-fed wearable antenna at ISM band for biomedical and WBAN applications," Wireless Networks, vol. 27, no. 1, pp. 735–745, Jan. 2021.

[3] G. Iddan, G. Meron, A. Glukhovsky, and P. Swain, "Wireless capsule endoscopy," Nature, vol. 405, May 2000, Art. no. 417.

[4] M. Zada, I. A. Shah, A. Basir, and H. Yoo, "Ultra-compact implantable antenna with enhanced performance for leadless cardiac pacemaker system," IEEE Trans. Antennas Propag., vol. 69, no. 2, pp. 1152–1157, Feb. 2021.

[5] S. A. A. Shah and H. Yoo, "Scalp-implantable antenna systems for intracranial pressure monitoring," IEEE Trans. Antennas Propag., vol. 66, no. 4, pp. 2170–2173, Apr. 2018.

[6] A. R. Chishti et al., "Advances in antenna-based techniques for detection and monitoring of critical chronic diseases: A comprehensive review," IEEE Access, vol. 11, pp. 104463–104484, 2023.

[7] A. Iqbal, M. Al-Hasan, I. B. Mabrouk, and T. A. Denidni, "Capsule endoscopic MIMO antenna with radiation pattern and polarization diversity," IEEE Trans. Antennas Propag., vol. 71, no. 4, pp. 3146–3154, Apr. 2023.

[8] A. J. Alazemi and A. Iqbal, "A high data rate implantable MIMO antenna for deep implanted biomedical devices," IEEE Trans. Antennas Propag., vol. 70, no. 2, pp. 998–1007, Feb. 2022.

[9] M. Khalid, M. Zahid, M. Yousaf, A. Akram, Y. Amin, and M. A. Qureshi, "An ultra miniaturized implantable antenna for gastrointestinal tract monitoring," in Proc. IEEE Int. Conf. Emerg. Trends Eng., Sci. Technol., 2023, pp. 1–5.

[10] A. Iqbal, M. Al-Hasan, I. B. Mabrouk, and M. Nedil, "Scalp-implantable MIMO antenna for high-data-rate head implants," IEEE Antennas Wireless Propag. Lett., vol. 20, no. 12, pp. 2529–2533, Dec. 2021.

[11] Make Madhu Manikya Kumar,Rama Devi Kolisetty “Compact Multi-Ring Reflect array Antenna at Wi-Fi for Overcoming Signal Blockage in Dense Urban Areas”,Progress In Electromagnetics Research C, Vol. 165, pp. 239–246, Feb 2026.

[12] A. Basir, M. Zada, Y. Cho, and H. Yoo, "A dual-circular-polarized endoscopic antenna with wideband characteristics and wireless biotelemetric link characterization," IEEE Trans. Antennas Propag., vol. 68, no. 10, pp. 6953–6963, Oct. 2020.

[13] A. Iqbal, M. Al-Hasan, I. B. Mabrouk, and M. Nedil, "A compact implantable MIMO antenna for high-data-rate biotelemetry applications," IEEE Trans. Antennas Propag., vol. 70, no. 1, pp. 631–640, Jan. 2022.

[14] S. N. Shah, M. Zada, J. Nasir, S. M. A. Shah, E. Arnieri, and H. Yoo, "Dual-band two-port MIMO antenna for biomedical deep tissue communication: Design, characterization, and performance analysis," IEEE Access, vol. 11, pp. 104622–104632, 2023.

[15] D. Sharma, R. N. Tiwari, B. K. Kanaujia, S. Kumar, and K. Rambabu, "Dual-band MIMO antenna data telemetry for dualchamber leadless cardiac pacing on Internet of Things environment," IEEE Internet Things J., vol. 11, no. 5, pp. 9072–9085, Mar. 2024.

[16] M. Zada and H. Yoo, "A miniaturized triple-band implantable antenna system for bio-telemetry applications," IEEE Trans. Antennas Propag., vol. 66, no. 12, pp. 7378–7382, Dec. 2018.

[17] K. Premchand, A. Jhansi Rani & K. Rama Devi ,“A corrugated edge tapered slot dual polarized MIMO antenna for phased array systems”International Journal of Electronics Volume 112, 2025 - Issue 10, pp.1362-3060 Nov. 2024.

[18] R. Ali, Y. Cho, I. A. Shah, S. Hayat, A. Basir, and H. Yoo, "Compact dual-band MIMO implantable antenna system for highdata-rate cortical visual prostheses applications," IEEE Trans. Antennas Propag., vol. 72, no. 8, pp. 6374–6386, Aug. 2024.

[19] IEEE Standard for Safety Levels With Respect to Human Exposure to Electric, Magnetic, and Electromagnetic Fields, 0 Hz to 300 GHz, IEEE Standard C95.1-2019, Oct. 2019.

[20] ANSYS Inc., "Ansys HFSS: High Frequency Electromagnetic Field Simulation Software," Ansys Electronics Desktop User Guide.

[21] Rogers Corporation, "RT/duroid 6010/6010LM High Frequency Laminates Data Sheet," Rogers Corp., Chandler, AZ, USA.

[22] T. Bashir, W. Li, and T. Xia, "Radiation Diversity Enabled Self-Isolated Compact Dual-Band Cubic MIMO Antenna for Wireless Biomedical Implants in Variable and Dynamic Environment," IEEE J. Microwaves, vol. 5, no. 5, pp. 1053–1070, Sep. 2025.